IET Renewable Power Generation

Special Issue Call for Papers

Be Seen. Be Cited.
Submit your work to a new IET special issue

Connect with researchers and experts in your field and share knowledge.

Be part of the latest research trends, faster.

Read more

The Institution of Engineering and Technology

Received: 12 August 2021 | Revised: 27 December 2021 | Accepted: 11 March 2022

IET Renewable Power Generation

DOI: 10.1049/rpg2.12454

The Institution of Engineering and Technology WILEY

ORIGINAL RESEARCH

Grid-forming inverter control design for PV sources considering DC-link dynamics

Ishita Ray[1] | **Leon M. Tolbert**[2]

[1]Center for Interdisciplinary Research and Graduate Education, The University of Tennessee, Knoxville, Tennessee, USA

[2]Department of Electrical Engineering and Computer Science, The University of Tennessee, Knoxville, Tennessee, USA

Correspondence
Ishita Ray, 444 Greve Hall, 821 Volunteer Blvd. Knoxville, TN 37996, USA.
Email: iray1@vols.utk.edu

Funding information
CURENT; Engineering Research Centers, Grant/Award Number: NSF Award Number EEC-1041877

Abstract

A grid-forming inverter in an inverter-dominated grid should operate as a dispatchable voltage source, which is difficult to achieve when the inverter is interfaced with nonlinear dc sources such as photovoltaic (PV) arrays. This paper presents a new grid-forming controller which considers the PV source dynamics and limitations and maintains dc-link stability under transient and overload conditions. A single-loop voltage controller without ac current feedback is used, and the synchronization is achieved using dc voltage-frequency droop. Additional dc current-virtual impedance feedforward compensation is included to improve the ac output passivity. The controller limits the operation of the PV source inverter in the linear portion of its characteristic by regulating its modulation index, thus preventing dc voltage collapse. The proposed controller is implemented and tested on a controller-in-the-loop simulation platform. The simulation results show that the controller shares power in proportion to the dc source capacities of parallel inverters, effectively limits the output current during faults, and limits dc-link voltage drop when the inverter is overloaded. The controller is also validated on a hardware testbed.

1 | INTRODUCTION

With movement from centralized generation and synchronous generators to distributed generation and renewable sources, inverters have transitioned from providing load support and ancillary services to now replacing synchronous generators as autonomous sources. These types of source inverters are commonly referred to as grid-forming inverters [1]. A grid-forming inverter can be used as the primary source in an isolated grid with multiple grid-following inverters or in parallel with other grid-forming inverters [2]. Clearly, having multiple grid-forming inverters in parallel eliminates the single point of failure and creates a more robust grid.

Nonetheless, disparate dc sources may be connected to these inverters, like energy storage and photovoltaic (PV) arrays [3]. The battery output voltage is determined by its state of charge whereas the PV output voltage is determined by its power point. In PV source control, Maximum Power Point Tracking (MPPT) control can either be applied to the duty cycle for open-loop control or the PV voltage for closed-loop control [4]. This makes the PV array a nonlinear current source which can operate in constant current mode below the MPP voltage, constant power mode around the MPP voltage, and constant voltage mode above the MPP voltage [5]. The current vs. voltage and power vs. voltage characteristics for a PV array with 1000 W/m^2 irradiation are shown in Figure 1.

The assumption of an infinite dc source upstream of a grid-tied inverter leads to the disregard of the behavior and dynamics of the dc source, dc-link capacitor, and dc/dc converter control. When there is a sudden change in load, the response of the dc source system will be determined by these three components [6]. A constant dc voltage regardless of loading conditions can only be maintained by a large energy storage (in the form of a capacitor or additional battery) on the dc-side [7] or ac-side [8], which adds to the cost and size of the system. PV generators with battery storage support and virtual synchronous generator (VSG) control are often used in islanded/isolated grids in both grid-following and grid-forming modes [9, 10]. In [11], to avoid the use of additional energy storage with a PV inverter, the PV source is operated below MPP to reserve power for frequency response. This grid-supporting PV inverter with VSG

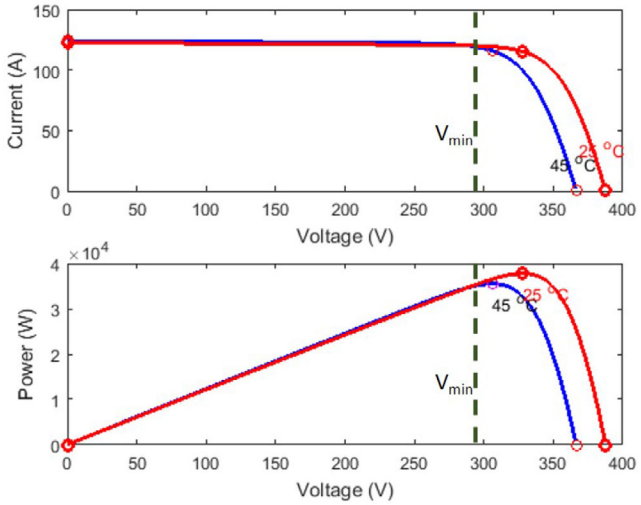

FIGURE 1 PV characteristics at 1000 W/m^2 for a 38 kVA PV generator

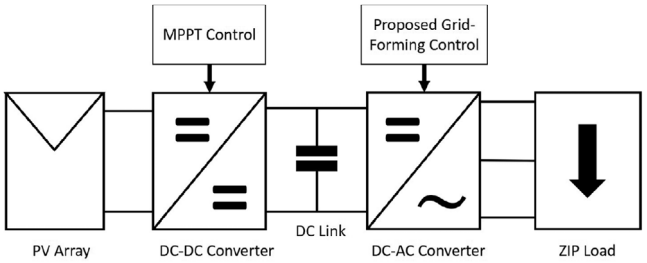

FIGURE 2 Two-stage PV source inverter system

control produces a lower dc voltage ripple when tracking frequency changes.

Although using a grid-forming battery system with a grid-feeding PV array is economical for islanded grids, the cost and size of this combination may hinder adoption by individual residential customers. In some cases, the PV and battery systems may have separate owners with individual grid-forming controllers that need to operate in parallel. In these cases, the ability to operate the PV source as an isolated dispatchable source will reduce costs and barriers to integration of PV sources for even the smallest consumers.

Therefore, the most efficient way to operate a PV source (at or near its maximum power point) is not always feasible. Although operating the inverter in voltage-fed mode may limit the dc voltage to values higher than the MPP voltage, restricting the voltage to this constant voltage region will avoid any unstable situations [12]. On the other hand, if the voltage is below the MPP and the PV source operates in the constant current region, the duty cycle will be decreased to maintain the output current. This lower duty cycle will further lower the output voltage to provide more current to the load, effectively reducing the PV power output. Therefore, the power characteristic below the MPP voltage is unstable and can cause the dc bus voltage to ultimately collapse [13].

This can happen even if the available PV power is higher than the load demand, and preventing this voltage collapse is the primary objective in designing a proper dc/ac inverter controller for a PV source with MPPT control. Ignoring the limitations of a practical dc source can result in a mismatch between input and output power, which will cause the dc voltage to drop and affect the performance of the inverter [14]. According to [15], the dc-link voltage should not drop below $2v_{ref}/1.1$ if the inverter output is to be maintained at the voltage level v_{ref}, with 1.1 being the maximum allowable modulation index.

As explained in [16], any inverter that interfaces a PV source with the grid should be able to protect the dc-link voltage from large load transients. This is not a concern in grid-following inverters where the dc-link voltage is regulated by the grid-following controller [17–19]. In the absence of a dc-link controller (in the grid-connected inverter or with additional storage at the dc-link), adjusting the PV power output lower than the maximum power point in the constant voltage region can protect the dc-link against ac-side transients. While exceeding the capability of the PV source will cause a voltage collapse, underloading the PV source will simply cause the PV source output to be reduced below its MPP [16]. This will not only prevent a voltage collapse in the PV array but also maintain sufficient dc-link voltage for PWM modulation. With this consideration, a single-loop grid-forming controller is developed that is capable of robust parallel operation and overcurrent protection while maintaining a stable dc-link voltage. This type of control improves the ride-through capability of the grid-forming sources during overload and fault conditions, thus enhancing the resiliency of the isolated grid.

The remainder of the paper is divided into four sections. Section 2 describes the proposed grid-forming controller and analyzes its stability based on the closed-loop inverter input and output impedances. Section 3 presents the simulation results for three test cases using the proposed controller in an inverter-based grid. Section 4 details the experimental setup used to validate the controller and presents the experimental results. The paper is concluded in Section 5.

2 | GRID-FORMING CONTROL DESIGN

This section will describe the control design of a grid-forming controller for an MPPT-controlled PV source. An effective grid-forming inverter controller should:

- sufficiently decouple dc and ac dynamics
- be impervious to changing grid conditions in terms of synchronization and power sharing with other inverters
- protect the inverter during transient events without losing stability
- have stable ac output while maintaining dc-link stability
- have minimum interaction with other inverter controllers and thereby, have minimum impact on their stability

The PV source is connected to the load through a two-stage inverter system comprised of a dc-dc boost converter and a dc/ac power inverter as presented in Figure 2. The circuit model

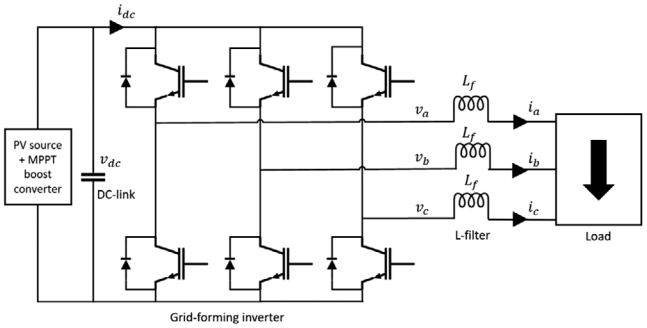

FIGURE 3 Circuit model of grid-forming inverter with L-filter

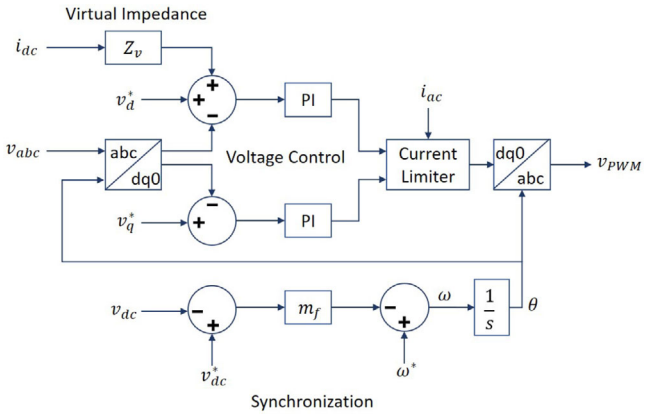

FIGURE 4 Proposed grid-forming controller

of the grid-forming inverter interfaced with an L-filter is shown in Figure 3 with the proposed controller shown in Figure 4. The boost converter is controlled using a perturb-and-observe MPPT algorithm, and the power inverter is controlled using the grid-forming method described below. Although a two-stage inverter has lower efficiency, it improves MPPT efficiency and expands the operation range compared to a single stage inverter. Also, the dc-dc converter prevents ac power ripple from harming the dc source [18].

2.1 | AC voltage control

Researchers have found certain drawbacks to using inner current control loops in power electronics-based machine emulators which can pertain to grid-connected inverters as well. According to [20], the inner current control loop can:

- act as a low pass filter that distorts the voltage output during load transients
- reduce the emulation accuracy when the electrical machine frequency is close to or higher than the current loop bandwidth
- decrease the phase margin and in turn, the stability of the system during transient conditions

The comparative analysis of single and nested loop controllers in [21] also displays how the use of inner (current) control loops leads to negative resistance behavior in the input impedance and non-passive regions in the output impedance of grid-forming inverters. Therefore, a single-loop voltage controller can provide enhanced dc and ac stability by evading these issues and minimizing the negative resistance behavior on the dc side. The analysis in [21] was used as the basis for designing the proposed single-loop grid-forming controller.

In the proposed controller, the PWM signal is derived from a single proportional integral (PI) control loop with d-axis and q-axis voltage measurements (v_d, v_q) as feedback and d-q references (v_{d-ref}, v_{q-ref}) set to 1 p.u. and can be described using these equations:

$$v_{d-PWM} = k_p(v_{d-ref} - v_d) + k_i \int_0^t (v_{d-ref} - v_d)dt, \quad (1)$$

$$v_{q-PWM} = k_p(v_{q-ref} - v_q) + k_i \int_0^t (v_{q-ref} - v_q)dt, \quad (2)$$

where k_p and k_i are the proportional and integral gains, respectively. These gains were tuned by analyzing the output response of the simulated system.

2.2 | DC current feedforward for improving passivity

While this single-loop control does not provide implicit current limiting, it has higher control bandwidth than a dual-loop controller and prevents negative resistance behavior in the input and output impedance, which will be revealed by the stability analysis later in this section. Nevertheless, the passivity of the inverter system (which is affected by resonances caused by the output impedance) can be further improved by adding a dc current feedforward (i_{dc}) with virtual impedance Z_v to the voltage control reference such that the new reference v'_{ref} (for respective axis) becomes:

$$v'_{ref} = v_{ref} + Z_v i_{dc}. \quad (3)$$

Here, a resistive-capacitive (R-C) virtual impedance is used in the dc current feedforward loop since it provides minimum voltage distortion and improved harmonic current sharing among parallel inverters. Furthermore, using dc current feedforward avoids the positive feedback effect that can arise from using ac current which is affected by variations in grid impedance [22]. The R-C virtual impedance is designed using the method provided in [23].

2.3 | DC voltage- AC frequency droop

DC-link voltage is as important to dc-side dynamics as frequency stability is to the ac-side dynamics. Hence, it is

reasonable to link them through the control action. Similar to matching control [24], this synchronization loop uses dc-link voltage (v_{dc}) to derive the frequency and phase angle of the PWM output as follows:

$$\omega = \omega^* - m_f(v_{dc}^* - v_{dc}), \tag{4}$$

where m_f is the droop coefficient, ω^* is the frequency reference, and v_{dc}^* is the dc voltage reference. For a limited dc source, the dc-link voltage is not impervious to changes in loading conditions and can be used as a measure of power balance by detecting the variation from the nominal value. In this way, any large drop in dc-link voltage will affect the output frequency instead of being disregarded. Unlike other grid-forming controllers, this type of controller includes the impact of dc-side disturbances on the output modulation rather than compensating for them until the dc-link voltage collapses.

2.4 | Regulating modulation index for overcurrent limitation

The analysis in [25] shows that unbalanced grid faults can create dc-link voltage oscillations and degrade the ride-through ability and grid support voltage functions. The controller in [25] is used to reject the dc-link oscillations and provide maximum fault current to support the grid voltage rather than to reduce the dc-link oscillations. However, the design objective of the proposed controller is not to ignore the dc-link oscillations and provide maximum fault current but rather to stabilize the dc-link and limit the output current within a safe range.

As mentioned earlier, battery storage systems are commonly used with PV arrays to maintain a stable dc-link voltage in grid-forming operation. If the dc-link is not maintained by additional storage, its voltage then depends on the PV output and can be severely affected by transient events. In the absence of an inner current control loop, the inductor current (i_g) can be used to adjust the modulation index in case of transient events. In the current limitation block, when the ac current passes a set threshold, the duty cycle is reduced in proportion to the increase in current:

$$v'_{PWM} = \begin{cases} v_{PWM}, & \text{if} \quad i_{ac} \le I_{limit} \\ \left(\frac{I_{limit}}{i_{ac}}\right) v_{PWM}, & \text{if} \quad i_{ac} > I_{limit} \end{cases}, \tag{5}$$

where v_{PWM} is the original PWM reference, v'_{PWM} is the modified PWM reference, and i_{ac} is the ac current feedback. Here, the I_{limit} is not the inverter overcurrent limit but is the current corresponding to V_{min} point on the MPP curve in Figure 1. The adjustment of the modulation index is saturated between the index limits set to ensure the output voltage does not drop below a certain value for ride-through purposes while maintaining sufficient overload capability. This enables the controller to not only limit the output current but to also stabilize the dc-link.

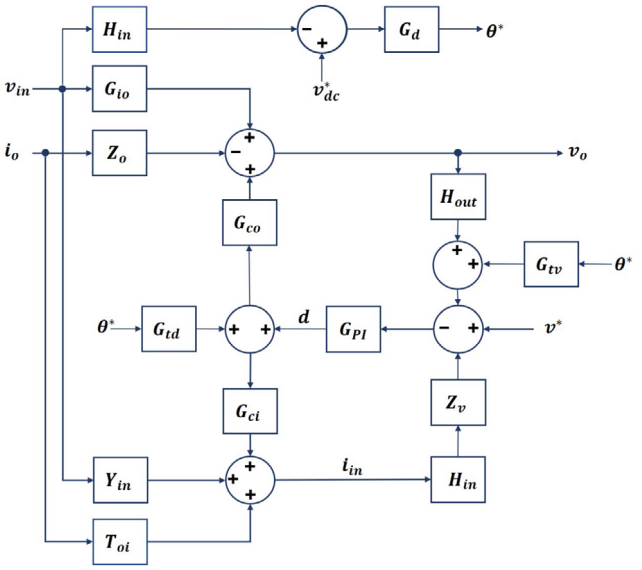

FIGURE 5 Transfer function representation of input and output dynamics for grid-forming inverter

TABLE 1 Grid-forming converter and controller parameters

Nominal voltage	480 V
Nominal load	5 kW, 2.5 kVar
Nominal frequency	60 Hz
PV rated power	24 kVA
BESS rated power	10 kVA
L-filter: L, R_l	0.1 mH,10 mΩ
Dc-link capacitor	6.7 mF
Droop curve gain: m_f	0.01
Sampling period: T_s	100 μs
Switching frequency: f_{sw}	10 kHz
PI controller gains: k_p, k_i	0.3, 8
Filter frequency: ω_f	1500 Hz
Virtual impedance: R_v, C_v	1.25 Ω, 0.1 mF

2.5 | Impedance analysis of converter controller

Impedance analysis of the inverter control system provides useful insights into the impact of the controller design on the dc and ac dynamics of the system [26]. The grid-forming inverter is modeled as a voltage-source voltage-output inverter as represented in Figure 5. Following the methodology in [27], this representation is used to derive the open-loop and closed-loop input admittance and output impedance functions with _o denoting open-loop, _c denoting closed-loop without virtual impedance feedforward, and _cv denoting closed-loop with virtual impedance feedforward. The system and controller parameters used for the analysis are provided in Table 1.

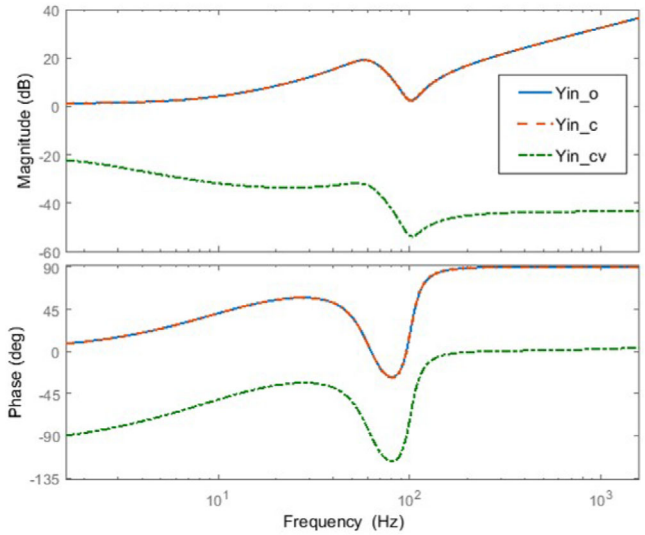

FIGURE 6 Bode plot of inverter input (dc) admittance

$$Z_{o\_c} = \frac{Z_{o\_o}}{I + G_{co}G_{PI}H_{out}}, \tag{6}$$

$$Y_{in\_c} = Y_{in\_o} - G_{ci}(G_{PI}G_{tv} + G_{td})G_dH_{in}, \tag{7}$$

$$Z_{o\_cv} = \frac{Z_{o\_o} + G_{co}G_{PI}Z_vH_{in}T_{oi}}{I + G_{co}G_{PI}H_{out}}, \tag{8}$$

$$Y_{in\_cv} = \frac{Y_{in\_o} - G_{ci}(G_{PI}G_{tv} + G_{td})G_dH_{in}}{I + G_{ci}G_{PI}Z_vH_{in}}. \tag{9}$$

In these equations: Z_o is the output (ac) impedance, Y_{in} is the input (dc) admittance, H_{in} and H_{out} are the input and output control delay respectively, G_{io} is the input to output (dc to ac) voltage loop gain, T_{oi} output to input (ac to dc) current loop gain, G_{ci} and G_{co} are the inner and outer control loop gain respectively, G_{PI} is the PI control gain for the voltage control loop, G_{tv} and G_{td} are the phase angle to voltage and phase angle to duty cycle gain respectively, and $G_d = G_{filter}m_{dc}G_s$ is the droop control loop gain with G_{filter} being the low-pass filter gain, m_{dc} being the droop coefficient and G_s is the integral gain.

The impedance equations along with the parameters are coded into MATLAB to produce the input and output impedance plots. The open-loop impedance values are calculated from the state space equations of the equivalent circuit of the grid-forming inverter:

$$\begin{bmatrix} v_{in} \\ i_o \end{bmatrix} = \begin{bmatrix} Z_{in} & T_{oi} & G_{ci} \\ G_{io} & Y_o & G_{co} \end{bmatrix} \cdot \begin{bmatrix} i_{in} \\ v_o \\ d \end{bmatrix}. \tag{10}$$

Figure 6 shows that the closed-loop input admittance of the inverter is not affected by the voltage control or the synchronization loop and behaves as a passive capacitance, similar to the open-loop admittance. The addition of the virtual impedance feedforward has an overall inductive effect but the dc-link is designed to be passive and stable. The dip around 90 Hz in these plots is a result of the control delay.

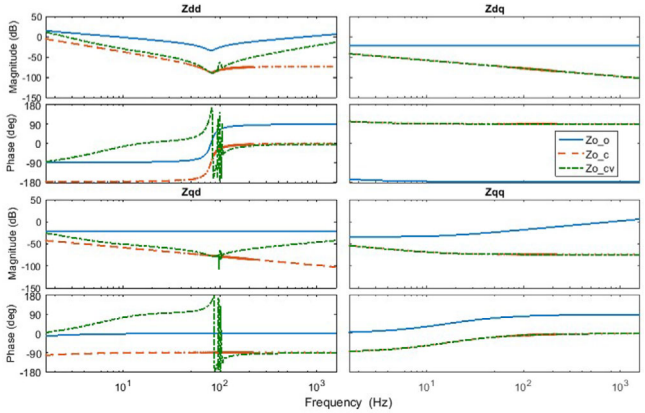

FIGURE 7 Bode plot of inverter output (ac) impedance

Figure 7 shows the effect of the voltage control, synchronization control, and virtual impedance feedforward control on the closed-loop output impedance of the grid-forming inverter. As expected, the d-axis and q-axis closed-loop output impedances are larger with higher coupling magnitudes between the axes. However, the single control loop without virtual impedance renders the d-axis impedance non-passive at lower frequencies, while the q-axis impedance remains passive throughout. Therefore, the virtual impedance feedforward is added along the d-axis to improve passivity. The controller with virtual impedance feedforward makes the output impedance passive everywhere except for the resonance point (caused by control delays) around 90 Hz. The bandwidth of this controller would increase to be around 900 Hz with the addition of an inner control loop. The feedforward control also reduces the cross-coupling magnitude in Z_{qd}. Hence, the q-axis impedance is passive both with and without virtual impedance, but the d-axis impedance becomes more passive at lower frequencies with the inclusion of virtual impedance. This improvement in passivity ensures that the controller is less sensitive to external disturbances.

3 | SIMULATION RESULTS WITH PROPOSED GRID-FORMING CONTROLLER

The simulation is performed on an Opal-RT platform with a controller in the loop (CIL). The grid-forming controller is implemented in a NI cRIO 9039, and the rest of the system is simulated in a Simulink model. Figure 8 shows the single-line representation of the Simulink model deployed on the Opal-RT platform. The proposed controller is deployed in both the PV and BESS source inverters, which are connected to the the two loads through L-filters. The grid impedance has an X/R ratio of 1. The PV system has a constant irradiance of 1000 W/m^2 and

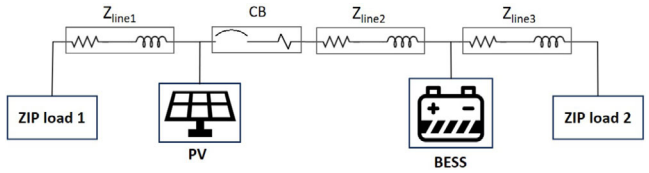

FIGURE 8 Simulink model of inverter-based grid with parallel PV and BESS grid-forming inverters

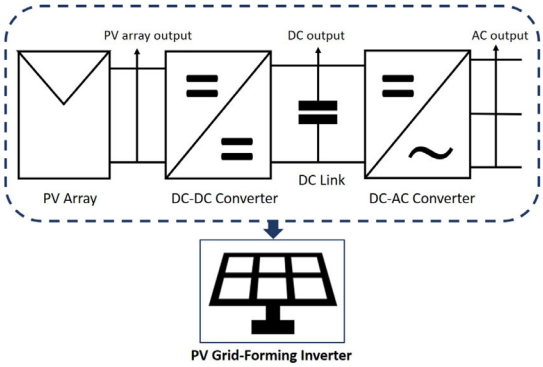

FIGURE 9 Composition of PV block in Simulink model

temperature of 40∘C. The PV array uses a single diode model with a temperature- and light-dependent current source, diode, and series and shunt resistances. The energy storage system uses a generic battery model and has a default state-of-charge (SoC) of 60%.

The BESS unit is also a two-stage inverter system with average models used to simulate the converters. While both PV and BESS sources have the same grid-forming inverter control, the BESS uses closed-loop dc voltage control at the dc boost converter stage while the PV source uses MPPT. The ZIP load is modeled using three single-phase current sources and has adjustable ZIP coefficients and active-reactive power setpoints. The ZIP loads are comprised of 30% Z-load (constant impedance), 30% I-load (constant current), and 40% P-load (constant power). The system and control parameters are the same as those used for the impedance analysis in Table 1. Three test cases are used to assess the performance of the grid-forming controller.

In Figure 8, the PV array, dc-dc converter, and dc-ac converter are combined in the PV grid-forming inverter block, as shown in Figure 9. For the following results, PV array voltage is measured at the output of the PV array, the dc-link voltages are measured at the dc link between the two converters, and the ac voltages and currents are measured at the output of the dc-ac converter.

3.1 | Parallel operation

The two inverters in Figure 8 are operated in parallel to test their synchronization stability as well as their power sharing capabilities. Before the circuit breaker closes to connect the PV and BESS sections at 2 s, the two ZIP loads operate separately with a nominal load of 5 kW and 2.5 kVar. Without changing the loads, when the two sections are connected at 2 s, the inverter ac voltages in Figure 10a are unaffected but the PV picks up more load from the BESS section, as shown from the ac current results in Figure 10b.

This can be explained by the dc voltage results in Figure 10c. When the PV is only supporting ZIP load 1, the dc-link voltage is modulated to slightly above 1 p.u. which shows that the PV inverter capacity is underutilized. As the two sources try to synchronize their output frequencies using the dc voltage-frequency droop control, their dc-link voltages settle at the same level. Unlike the BESS dc voltage which is not affected by shedding a portion of its load, the PV dc voltage drops closer to the BESS dc voltage when it picks up more load. Even though the PV source is still operating in the constant voltage region, it moves slightly closer to the MPP to pick up the additional load and balance its dc voltage with that of the BESS. The amount of additional load that can be picked up by the PV is determined by the PV source capacity as well as the line impedance. In this way, the two inverters are able to share power in proportion to their source capacities rather than sharing the loads equally.

Although in grid-forming controllers, the active and reactive power outputs are not directly controlled (unlike grid-following controllers), the voltage and frequency control laws can affect how power is shared between parallel inverters. For constant voltage sources, the dc-link voltage is directly related to the available output capacity of the source and hence, by linking the dc-link voltage to frequency synchronization, the output is controlled not by how much power is demanded by loads but rather by how much power is available at the source.

3.2 | Balanced three-phase fault

A balanced three-phase fault is simulated in a single-inverter system, depicted in Figure 11 to test the current limiting capability of the proposed controller in the PV inverter. The fault occurs at 1 s and is cleared at 1.2 s. Without any current limiting in Figure 12, the ac voltage drops to 0.75 p.u. and the dc voltage drops to 0.7 p.u. The ac current transient reaches 2.5 p.u. before settling around 2 p.u. (when PV inverter is overloaded). The PV source output voltage also suffers a 20% drop and moves into the constant current region of MPPT operation, which can make grid-forming operation unstable if the fault persists (assuming the inverter overcurrent protection is not triggered).

On the other hand, in Figure 13, the grid-forming controller with current limiting is able to limit the current below 2 p.u. without overloading the PV source. Although the ac output voltage drops to 0.5 p.u., the drop is not sufficient to trigger low-voltage ride-through protection in the inverter. The drop in dc-link and PV source output voltage are less than 10%, which means that the PV source remains around the (stable) maximum power point. However, for a lower fault impedance, the current limiting would not be able to limit the current to the same value

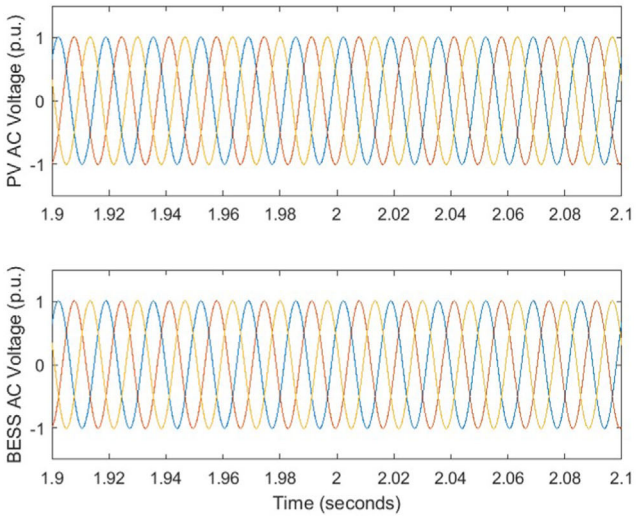

(a) Inverter output voltage

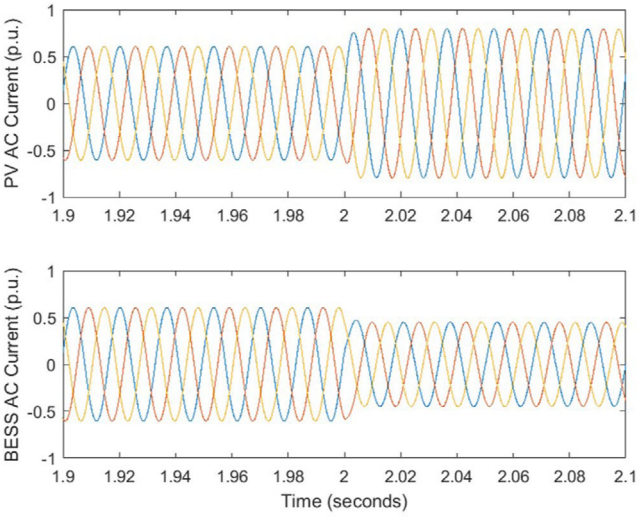

(b) Inverter output current

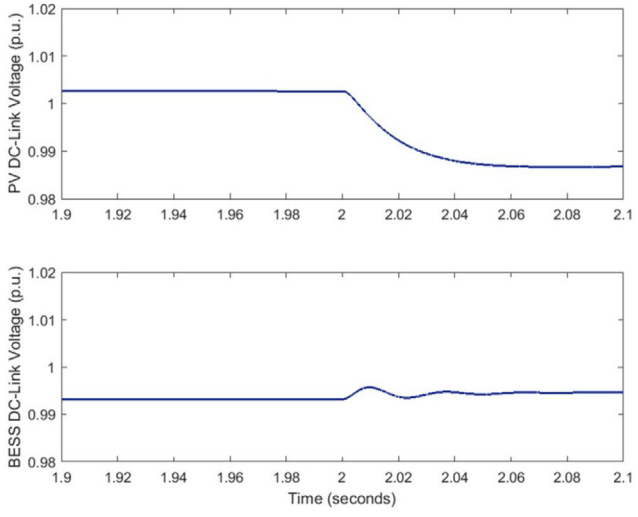

(c) DC-link voltage

FIGURE 10 Voltage and current waveforms for parallel operation of PV and BESS inverters

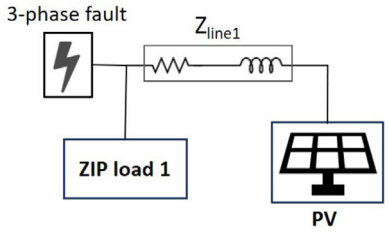

FIGURE 11 Simulink model of PV grid-forming inverter with 3-phase fault

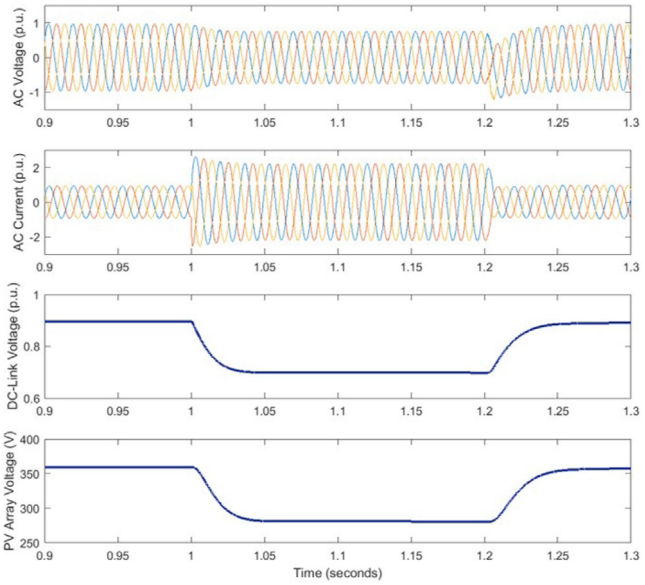

FIGURE 12 Results for inverter control without current limiting during a three-phase fault

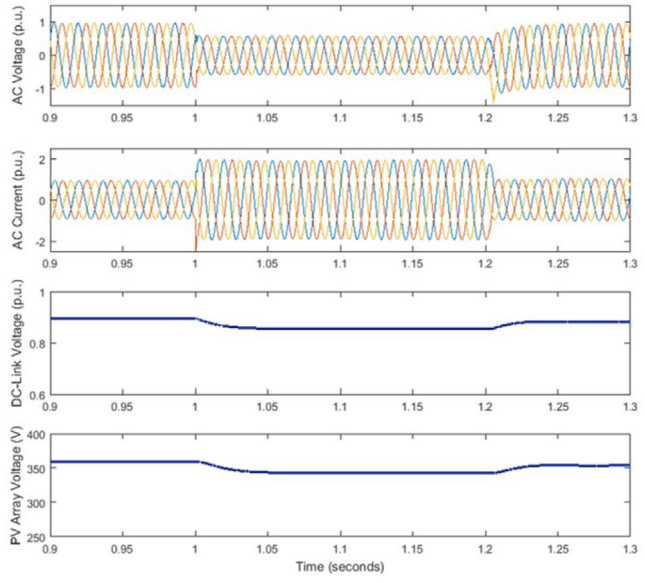

FIGURE 13 Results for inverter control with current limiting during a three-phase fault

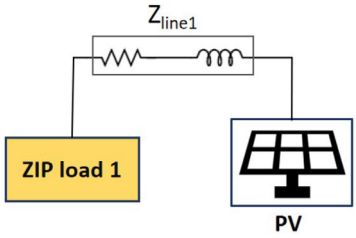

FIGURE 14 Simulink model of PV grid-forming inverter with changing load

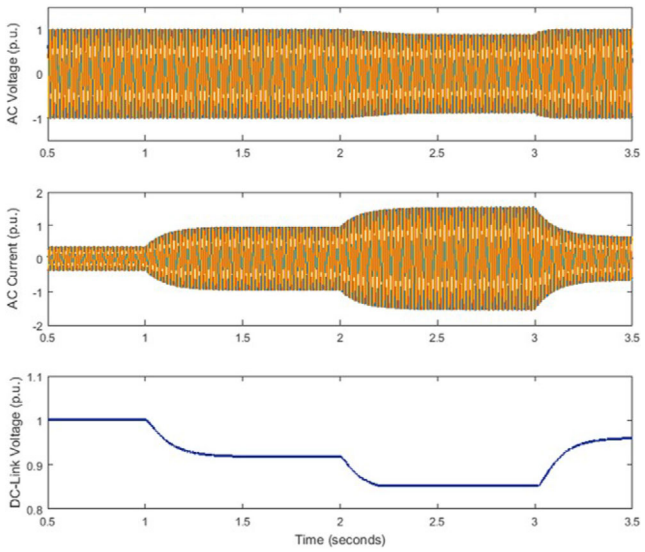

FIGURE 15 Results for step increase in load with proposed controller

without further decreasing the ac voltage. Nevertheless, limiting the current during faults protects both the inverter and the PV source.

3.3 | Step load change

This scenario is also simulated in a single-inverter system as presented in Fig 14. In this test case, ZIP load 1 active power setpoint is increased at every second in steps of 0.3 p.u. starting from the nominal load of 0.6 p.u. (5 kW) as shown in Figure 15. The proposed controller is able to accommodate an additional 0.3 p.u. of load without any effect on the ac voltage but with an 8% drop in the dc-link voltage. However, with an additional 0.6 p.u. of load, the PV source becomes overloaded. At this point, the dc-link voltage drops another 8%, which is below the required dc voltage level to maintain PWM modulation. Therefore, the ac voltage drops to 0.9 p.u. When the current is reduced below 1 p.u., the ac voltage level returns to 1 p.u. The drop in dc-link voltage is proportional to the difference in ac power output and available dc power. This demonstrates the limited extent to which the PV source can be exploited to have ideal voltage source characteristics.

TABLE 2 Experimental setup parameters

Nominal ac voltage: V_{ac}	40 V (peak)
Nominal ac current: I_{ac}	27.44 A
Nominal dc voltage: V_{dc}	1000 V
L-filter inductor, resistor: L_f, r_f	0.575 mH, 0.2 Ω
Controller gains: k_p, k_i	0.105, 35

3.4 | Discussion

When closed-loop dc voltage control is used for the dc-dc boost converter of a voltage source like BESS, the dc-link voltage is dependent solely on the battery state of charge. Whereas, when a nonlinear current source like PV is controlled using MPPT, the PV array output voltage as well as the dc-link voltage are dependent on the loading conditions and can vary significantly. Outside the constant voltage region, ac voltage regulation is not only affected by the dc-link voltage dropping below $2v_{ref}/1.1$ but also by the increase in load as:

$$\Delta v_{ac} = -\frac{P_{PV}}{\Delta i_{ac}}, \tag{11}$$

where P_{PV} is the PV source output and i_{ac} is the ac current. When the PV voltage drops below the MPP voltage, the PV output power starts decreasing. This means that the amount of ac voltage drop relative to increase in ac current also reduces with the highest drop occurring at MPP. Therefore, if the PV voltage (and in turn the dc-link voltage) is restricted to the MPP level, the drop in ac voltage will be higher than when the dc voltage is slightly lower than the MPP voltage. This trade-off can be addressed by using the modulation index modifier to not only provide overcurrent protection but to also limit the dc voltage to some point below the MPP (in the constant current region) so as to maintain stable ac and dc voltage regulation during overload conditions.

4 | EXPERIMENTAL VALIDATION

The controller is also tested in a two-converter system on the CURENT hardware testbed [28] in a scaled-down version of the simulation system. One converter is controlled as the source inverter with PV emulation while the other converter is controlled as a ZIP load. The two converters are connected to a common dc supply and have identical L-filters on the ac side, as shown in Figure 16. The system and controller parameters are presented in Table 2. The PWM generation method is depicted in Figure 16b.

The proposed grid-forming controller is implemented in the source inverter and subjected to a step load change from 0.6 p.u. to 0.8 p.u. The dc voltage as well as the ac voltages and currents during the load change are captured using an oscilloscope and presented in Figure 17a, and Figure 17b presents the results for the same case of load change in the simulation

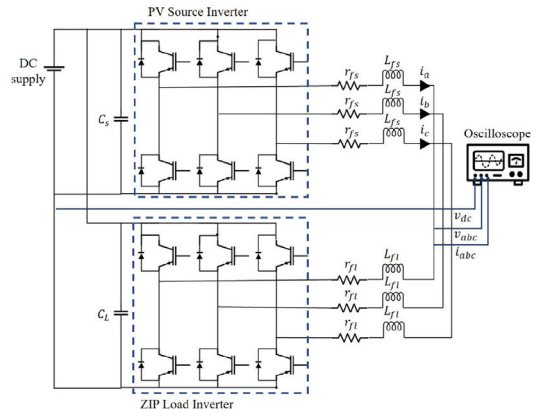

(a) Experimental setup schematic

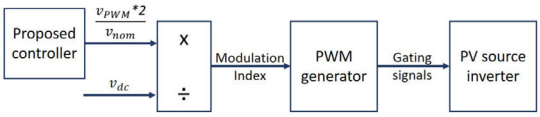

(b) PWM generation in hardware

(c) CURENT Hardware Testbed cabinet with inverters and filters

FIGURE 16 Experimental setup for testing grid-forming controllers

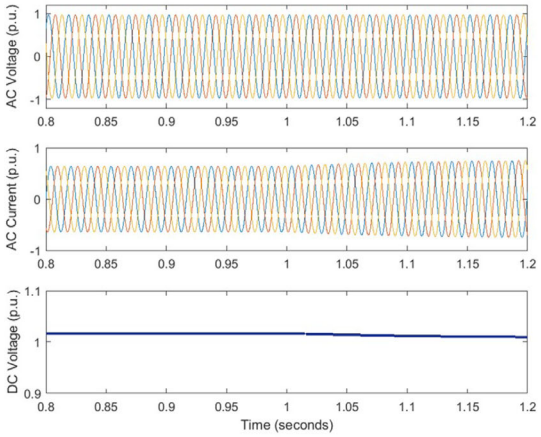

(a) Simulation results

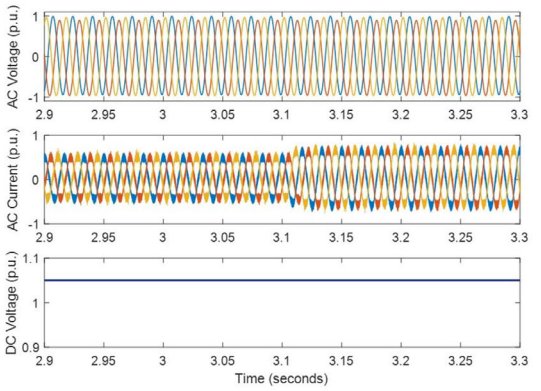

(b) Experimental results

FIGURE 17 Results for step change in load using the proposed grid-forming controller in simulation and hardware platforms

system used earlier. Both the experimental and simulation results show that during the load change, both the dc and ac voltages remain stable and unaffected as the current output increases.

Hence, the inverter does not experience any significant drop in the dc or ac voltage for a small change in load. However, a larger step change will cause a significant drop in the dc voltage for all load levels higher than 0.2 p.u. The ac voltage will remain unaffected until 2 p.u. which is when the PV source moves past its MPP. Any increase in load past this point will cause a drop in ac voltage that is proportional to the drop in dc voltage.

5 | CONCLUSION

This paper shows how a PV source can be utilized as a truly dispatchable voltage source by limiting its operation in the constant voltage region and not following the maximum power point curve until collapse. The proposed grid-forming controller is designed to maintain the PV output voltage close to the constant voltage region and prevent a dc-link voltage collapse, using a single-loop voltage control with overcurrent limiting. DC-voltage-frequency droop is used for frequency regulation, and the current is limited by adjusting the modulation index. The modulation index modifier used to limit overcurrent allows the PV inverter to have sufficient overload capability while restricting the PV voltage to a higher value in the constant current region. The simulation and experimental results show that the proposed controller is able to:

1. Synchronize parallel inverters with proportional load sharing
2. Limit overcurrent during transient events without sacrificing dc-link stability
3. Maintain dc-link stability when the source inverter is overloaded
4. Achieve passivity in input and output dynamics

Hence, by considering the limitations of the dc-link and the dc source behind the inverter, the proposed controller proves to be more suitable to connect a PV source with a dispatchable grid-forming inverter without additional storage at the dc-link.

ACKNOWLEDGEMENTS

The authors would like to acknowledge the support provided by Yiwei Ma in setting up the hardware testbed, troubleshooting and recording the experiments as well as Dingrui Li for providing additional laboratory support. This work was supported primarily by the ERC Program of the National Science Foundation and DOE under NSF Award Number EEC-1041877 and the CURENT Industry Partnership Program.

CONFLICT OF INTEREST

The authors have no conflicts of interest to declare.

PERMISSION TO REPRODUCE MATERIALS FROM OTHER SOURCES

None

DATA AVAILABILITY STATEMENT

Data sharing is not applicable to this article as no new data were created or analyzed in this study.

ORCID

Ishita Ray https://orcid.org/0000-0002-5080-0992

REFERENCES

1. Unruh, P., Nuschke, M., Strauß, P., Welck, F.: Overview on grid-forming inverter control methods. Energies 13(10), 2589 (2020)
2. Mirafzal, B., Adib, A.: On grid-interactive smart inverters: Features and advancements. IEEE Access 8, 160526–160536 (2020)
3. Díaz, N.L., Coelho, E.A., Vasquez, J.C., Guerrero, J.M.: Stability analysis for isolated ac microgrids based on pv-active generators. In: IEEE Energy Conversion Congress and Exposition (ECCE), pp. 4214–4221. IEEE, Piscataway (2015)
4. Messo, T., Puukko, J., Suntio, T.: Effect of MPP-tracking dc/dc converter on VSI-based photovoltaic inverter dynamics. In: 6th IET International Conference on Power Electronics, Machines and Drives (PEMD 2012), pp. 1–6. IET, Stevenage (2012)
5. Nousiainen, L., Puukko, J., Mäki, A., Messo, T., Huusari, J., Jokipii, J., et al.: Photovoltaic generator as an input source for power electronic converters. IEEE Trans. Power Electron. 28(6), 3028–3038 (2013)
6. Mäki, A., Valkealahti, S., Suntio, T.: Dynamic terminal characteristics of a photovoltaic generator. In: Proceedings of 14th International Power Electronics and Motion Control Conference EPE-PEMC, pp. 76–80. IEEE, Piscataway (2010)
7. Nikkhajoei, H., Lasseter, R.H.: Distributed generation interface to the CERTS microgrid. IEEE Trans. Power Delivery 24(3), 1598–1608 (2009)
8. Yazdani, S., Ferdowsi, M., Davari, M., Shamsi, P.: Advanced current-limiting and power-sharing control in a pv-based grid-forming inverter under unbalanced grid conditions. IEEE J. Emerg. Sel. Topics Power Electron. 8(2), 1084–1096 (2020)
9. Quan, X., Yu, R., Zhao, X., Lei, Y., Chen, T., Li, C., et al.: Photovoltaic synchronous generator: Architecture and control strategy for a grid-forming PV energy system. IEEE J. Emerg. Sel. Topics Power Electron. 8(2), 936–948 (2020)
10. Liu, J., Yang, D., Yao, W., Fang, R., Zhao, H., Wang, B.: PV-based virtual synchronous generator with variable inertia to enhance power system transient stability utilizing the energy storage system. Protection and Control of Modern Power Systems 2(38), 39 (2017)
11. Bao, G., Tan, H., Ding, K., Ma, M., Wang, N.: A novel photovoltaic virtual synchronous generator control technology without energy storage systems. Energies 12(12), 2240 (2019)
12. Suntio, T., Huusari, J., Leppäaho, J.: Issues on solar-generator interfacing with voltage-fed MPP-tracking converters. Eur. Power Electron. Drives 20(3), 40–47 (2010)
13. Viinamäki, J., Kuperman, A., Suntio, T.: Grid-forming-mode operation of boost-power-stage converter in PV-generator-interfacing applications. Energies 10(7), 1033 (2017)
14. Sitbon, M., Leppäaho, J., Suntio, T., Kuperman, A.: Dynamics of photovoltaic-generator-interfacing voltage-controlled buck power stage. IEEE J. Photovoltaics 5(2), 633–640 (2015)
15. Divshali, P.H., Alimardani, A., Hosseinian, S.H., Abedi, M.: Decentralized cooperative control strategy of microsources for stabilizing autonomous VSC-based microgrids. IEEE Trans. Power Syst. 27(4), 1949–1959 (2012)
16. Erickson, M.J., Jahns, T.M., Lasseter, R.H.: Comparison of PV inverter controller configurations for CERTS microgrid applications. In: IEEE Energy Conversion Congress and Exposition, pp. 659–666. IEEE, Piscataway (2011)
17. Du, W., Jiang, Q., Erickson, M.J., Lasseter, R.H.: Voltage-source control of PV inverter in a CERTS microgrid. IEEE Trans. Power Delivery 29(4), 1726–1734 (2014)
18. Gao, F., Li, D., Loh, P.C., Tang, Y., Wang, P.: Indirect dc-link voltage control of two-stage single-phase PV inverter. In: IEEE Energy Conversion Congress and Exposition (ECCE), pp. 1166–1172. IEEE, Piscataway (2009)
19. Cha, H., Lee, S.: Design and implementation of photovoltaic power conditioning system using a current based maximum power point tracking. In: IEEE Industry Applications Society Annual Meeting, pp. 1–5. IEEE, Piscataway (2008)
20. Ma, K., Song, Y.: Power-electronic-based electric machine emulator using direct impedance regulation. IEEE Trans. Power Electron. 35(10), 10673–10680 (2020)
21. Ray, I., Tolbert, L.M.: Small-signal impedance analysis of the impact of grid-forming controllers on their dc and ac dynamics. In: IEEE 12th International Symposium on Power Electronics for Distributed Generation Systems (PEDG), pp. 1–8. IEEE, Piscataway (2021)
22. Wang, J., Song, Y., Monti, A.: A study of feedforward control on stability of grid-parallel inverter with various grid impedance. In: IEEE 5th International Symposium on Power Electronics for Distributed Generation Systems (PEDG), pp. 1–8. IEEE, Piscataway (2014)
23. Micallef, A., Apap, M., Spiteri Staines, C., Guerrero, J.M.: Selective virtual capacitive impedance loop for harmonic voltage compensation in islanded microgrids. In: IECON 2013-39th Annual Conference of the IEEE Industrial Electronics Society, pp. 7968–7973. IEEE, Piscataway (2013)
24. Arghir, C., Jouini, T., Dörfler, F.: Grid-forming control for power converters based on matching of synchronous machines. Automatica 95, 273–282 (2018)
25. Just, H., Gentejohann, M., Eggers, M., Dieckerhoff, S.: Analysis and control of dc-link oscillations of voltage source inverters during unbalanced grid faults. In: 21st European Conference on Power Electronics and Applications, pp. 1–10. Springer, Berlin (2019)
26. Ray, I.: Review of impedance-based analysis methods applied to grid-forming inverters in inverter-dominated grids. Energies 14(9), 2686 (2021)
27. Suntio, T., Messo, T., Puukko, J.: Dynamic modeling of three-phase inverters. In: Power Electronic Converters: Dynamics and Control in Conventional and Renewable Energy Applications, pp. 491–532. John Wiley & Sons, Ltd, Weinheim (2017)
28. Tolbert, L.M., Wang, F., Tomsovic, K., Sun, K., Wang, J., Ma, Y., et al.: Reconfigurable real-time power grid emulator for systems with high penetration of renewables. IEEE Open Access J. Power Energy 7, 489–500 (2020)

How to cite this article: Ray, I., Tolbert, L.M.: Grid-forming inverter control design for PV sources considering DC-link dynamics. IET Renew. Power Gener. 1–10 (2022). https://doi.org/10.1049/rpg2.12454